Available online at www.sciencedirect.com

SCIENCE DIRECT

Developmental Biology 282 (2005) 55–69

DEVELOPMENTAL BIOLOGY

www.elsevier.com/locate/ydbio

Sid4: A secreted vertebrate immunoglobulin protein with roles in zebrafish embryogenesis

P.J. diIorio[a,*], A. Runko[b], C.A. Farrell[a], N. Roy[b]

[a]*Division of Diabetes, University of Massachusetts Medical School, 373 Plantation Street, Suite 218, Worcester, MA 01605, USA*
[b]*Department of Biochemistry and Pharmacology, University of Massachusetts Medical School, Worcester, MA 01605, USA*

Received for publication 11 December 2004, revised 22 February 2005, accepted 23 February 2005

Abstract

The small members of the immunoglobulin superfamily (IGSF) are a molecularly diverse group of proteins composed solely of immunoglobulin domains. They may be secreted or tethered to the cell mebrane via GPI linkages and are proposed to have important functions in vivo. However, very few small IGSFs have been functionally characterized. During an ongoing in situ hybridization analysis of expressed sequence tags in zebrafish we identified *secreted immunoglobulin domain 4* (*sid4*), a gene encoding a soluble vertebrate protein composed solely of four immunoglobulin domains.

Throughout development, *sid4* is expressed in regions of the embryo undergoing active cell division and migration. Functional analysis using morpholino antisense oligonucleotides demonstrates that timing of gene expression is normal in morphants, but these embryos are smaller and exhibit defects in epiboly and patterning of axial and prechordal mesoderm. Analyses of *chordin*, *pax2*, *krox20*, and *dlx2* expression in morphants demonstrate that early brain patterning is normal but later organization of hindbrain neurons and development of cranial neural crest are perturbed.

Levels of apoptosis in morphants were normal prior to 90% epiboly, but were elevated after 10 h post-fertilization (hpf). Apoptosis does not account for early patterning defects of axial mesoderm, but likely contributes to overall reduction in embryo size. Phylogenetic analysis demonstrates that Sid4 is strikingly similar to the fibronectin binding Ig domains of Perlecan/HSPG2. Overall, our data demonstrate a fundamental role for *sid4*, possibly as a co-factor in extracellular matrix (ECM) interactions, in processes underlying tissue patterning and organogenesis in a vertebrate.

Keywords: Apoptosis; Development; Extracellular matrix; Gastrulation; Immunoglobulin; Morpholino; Morphogenesis; Zebrafish

Introduction

Proteins belonging to the IGSF are structurally diverse and have multiple evolutionary origins. All members utilize the immunoglobulin (Ig) domain to participate in processes that depend on protein interactions, such as co-receptors for growth factors (Mongiat et al., 2000), adhesion to cells and extracellular matrix (Rougon and Hobert, 2003; Vaughn and Bjorkman, 1996), pathfinding by axons (Panicker et al., 2003), and blood vessel branching (Rossant and Howard, 2002).

Unlike the large, multimeric members of the family, small IGSFs are composed solely of Ig domains. They may be secreted or tethered to the cell membrane via GPI linkages (Rougon and Hobert, 2003). The molecular diversity of the small IGSF subfamily has been documented in *Drosophila* (Nakamura et al., 2002) and *Caenorhabditis elegans* (Teichmann and Chothia, 2000) but very little is known about their in vivo functions. Two small Igs, *Drosophila* Beaten path (Beat) 1a and Hemolin, are secreted and act as anti-adhesives to disrupt cell–cell interactions

* Corresponding author. Fax: +1 508 856 4093.
E-mail address: philip.diiorio@umassmed.edu (P.J. diIorio).

0012-1606/$ - see front matter © 2005 Elsevier Inc. All rights reserved.
doi:10.1016/j.ydbio.2005.02.036

during motorneuron axon migration (Fambrough and Goodman, 1996) and hemocytic aggregation in response to bacterial infection (Bettencourt et al., 1997, 1999; Kanost et al., 1994; Sun et al., 1990), respectively. BeatIa and Hemolin are also necessary for normal embryo development (Bettencourt et al., 2002; Pipes et al., 2001).

During an ongoing in situ hybridization screen of zebrafish expressed sequence tags (ESTs), we identified *secreted immunoglobulin domain 4* (after *Sid1*, (Yoder et al., 2002)). *sid4* is a novel vertebrate gene that, like moth Hemolin (Sun et al., 1990), encodes a secreted protein composed of four Ig domains and contains no other conserved motifs. *sid4* mRNA is maternally provisioned and zygotically expressed throughout development in regions of the embryo containing actively dividing and migrating cells.

Suppression of Sid4 by morpholino injection causes defects in morphogenesis but not cellular differentiation. Morphant embryos are reduced in size and exhibit impaired epiboly and morphogenesis of axial and somitic mesoderm. Despite morphological similarities to ventralized Wnt and dorsalized BMP mutants, expression of *bmp4* and *chordin* is normal in 6 hpf morphants. At 10 hpf, the conclusion of gastrulation in zebrafish, morphants first exhibit elevated levels of apoptosis, suggesting that decreased cell viability is secondary to the morphogenetic defect.

Although *sid4* mRNA is ubiquitously expressed through 16 hpf, morphants exhibit spatially and temporally restricted defects in morphogenesis of axial and prechordal mesoderm. For example, at similar stages of development, patterning of axial mesoderm is disrupted while anterior migration of prechordal mesoderm is normal. Additionally, while early hatching gland development appears normal, later anterolateral spreading of these cells is inhibited.

Phylogenetic sequence analysis demonstrates that Sid4 is closely related to mouse *Perlecan/HSPG2* and shares significant similarity with the fibronectin binding Ig domains of this large, multimeric protein. These data, together with our analyses of somitic mesoderm, cranial neural crest, and branchiomotor neurons suggest that this novel, vertebrate member of the IGSF may function as a secreted receptor or cofactor with important roles in some ECM interactions during embryogenesis.

Methods

Fish maintenance

Wild type and transgenic embryos expressing green fluorescent protein under the control of an *Islet-1* enhancer (Higashijima et al., 2000) were collected from natural matings and reared in 1/3 Ringer's (Westerfield, 2000). Embryos were staged using morphological criteria up to 24 h post fertilization (hpf) and by time of development at 28.5°C thereafter (Kimmel et al., 1995).

Cloning and molecular characterization of sid4

IMAGE clone 3719398 was initially identified as the zebrafish homolog of HSPG2/Perlecan. However, our preliminary BLAST analyses of this clone and human HSPG2 (gi184426) against the zebrafish genome demonstrated that these are distinct genetic loci. *sid4* was selected for functional characterization because it appeared to be a novel, developmentally expressed gene located in a region of the zebrafish genome containing an abundance of uncharacterized, predicted genes (Sanger, Zv4).

Full-length *sid4* (GENBANK AY494978) was isolated from 60 hpf total RNA (RNeasy, Qiagen). AMV-GeneRacer (Invitrogen) was used to amplify 5′ and 3′ cDNA ends with the oligonucleotides 5′CGCCTCGCTGGAGCCCACATGAT3′ and 5′TGACGGTGCCGTTCTGACCATCGCTAA3′, respectively. Amplification products were cloned into pCRII (Invitrogen) and multiple clones sequenced. A consensus cDNA sequence and conceptual translation were obtained using SeqMan (DNASTAR v. 4.0). ClustalW was used to produce nucleotide and amino acid sequence alignments (Macvector v. 7.2). Full-length *sid4* is identical to the available sequences in 64 recently deposited AGENCOURT ESTs (e.g gi46159009).

In situ hybridization

pSport containing *sid4* was linearized with *Sal1* and *Not1* and digoxigenin-labeled probes transcribed with Sp6 (antisense) and T7 (sense) RNA polymerases, respectively. Additional RNA probes used were zebrafish *flh* (Talbot et al., 1995), *bmp4* (Hwang et al., 1997), *chordin* (Schulte-Merker et al., 1997), *unc-45* (Etheridge et al., 2002), *pax-2* (Krauss et al., 1991), *hgg-1* (Vogel and Gerster, 1997), *goosecoid* (gsc) (Schulte-Merker et al., 1994; Thisse et al., 1994), *krox-20* (Oxtoby and Jowett, 1993), and *dlx-2* (Akimenko et al., 1994). In situ hybridization was carried out as described previously (diIorio et al., 2002; Willett et al., 1997).

Morpholino design and microinjection

Eight exons for *sid4* were localized to linkage group 25 (Sanger Zv4). We identified nucleotide sequence corresponding to the first 52 amino acids of *sid4*, but to date these have not been mapped. Exon 5 and flanking introns were amplified by standard PCR from genomic DNA using the oligonucleotides 5′CTAGATCACTTACGAGATGATCTTTGCGTGAA3′ and 5′CCACAATCAGA-GATCTGCAGCTCTGGA3′. Products were cloned into pCRII (Invitrogen) and sequenced. To verify the specificity of morpholino-induced phenotypes, two morpholinos were designed against distinct regions of *sid4* mRNA. The morpholino 5′GAGCTGCTGTCTGGAGCTTCATCAT3′ (t-mo) was designed against the *sid4* translation start site and 5′TGGTGATGGTGTGTTTACC-GGAGGC3′ (s-mo) targets

a predicted splice donor site at the boundary of exon 5 and intron 5. The respective control morpholinos 5′ GACCTCCTGTCTGCAG-CTTGATGAT 3′ (t-co) and 5′TGCTGTTGGTGTCTTTACCCGACGC3′ (s-co) both contain 5 mismatched bases. Morpholinos were reconstituted to 1 mM in 1× Danieau's buffer (Gene Tools) and diluted in 1× Danieau's buffer containing 0.1% phenol red for injection into 1–2 cell embryos. Unless specified, s-mo was used because (1) both morpholinos exhibited comparable effects on epiboly and patterning of somitic mesoderm, prechordal mesoderm and blood, (2) unlike inhibiting translation, exon deletion is irreversible, and (3) RT-PCR can be used to assay for exon deletion from mRNA processed in vivo.

To assess the qualitative effects of s-mo on *sid4* mRNA, total RNA was extracted from 6 hpf s-co and s-mo embryos (RNeasy, Qiagen) and 500 ng used in standard RT-PCR (One-Step, Qiagen). The oligonucleotides 5′ATGATGAA-GCTCCAGACAGCAGCTCT3′ and 5′CTGTAATTAAGC-TTTGACCGTGACTCT3′ span the entire *sid4* mRNA. Amplification products were cloned into pCRII (Invitrogen) and multiple clones sequenced.

sid4 Overexpression

Full-length *sid4* was amplified from adult liver total RNA using 5′CAACCATCGATAGATCTGCCACCA-TGATGAAGCTCCAGACA3′ containing an introduced, consensus Kozak sequence (Kozak, 1987), and 5′CAA-CCGAATTCAGCTTTGACCGTGACTCTGCTGA3′. Amplification products were digested with *Cla*I and *Eco*RI and ligated into pCS2. Four independent clones of pCS2 containing full-length *sid4* were linearized with *Not*I and capped mRNA transcribed from each with Sp6 (mMessage Machine, Ambion; RiboMax mRNA synthesis, Promega). Individual mRNA samples were purified by a number of protocols including: Phenol extraction, RNA mini prep kit (Qiagen), Trizol extraction, and MegaClear column purification (Ambion). mRNA was re-suspended in sterile, RNase-free water and quality assessed on 1% agarose gels both before and after injection.

To assess in vivo expression of *sid4* mRNA, pools of one hundred 12-hpf embryos were injected with various constructs and lysed in 150 μL 1× Kamen Sample Buffer (BioRad). In addition to *sid4* mRNA, we injected supercoiled plasmid DNA used to synthesize *sid4* mRNA as a positive control for *sid4* translation. Embryo lysates and molecular weight markers were separated by SDS-PAGE and visualized with silver stain.

TUNEL staining

Embryos were injected with 150 μM s-mo and fixed for TUNEL staining at 6 hpf, 90% epiboly, and 10 hpf. These stages represent the onset of gastrulation, a period of active migration, and the end of gastrulation, respectively. TUNEL was performed as described (Barrallo-Gimeno et al., 2004) and was optimized in our lab to detect endogenous apoptosis in the lens of 24 hpf embryos.

Imaging

In situ hybridized and TUNEL stained embryos were post-fixed in 4% paraformaldehyde and cleared in 80% glycerol. Live embryos were mounted in 3% methylcellulose in 1/3 Ringer's saline (Westerfield, 2000). Digital images were acquired with a Nikon Eclipse E600 microscope equipped with Nomarski optics. Images were acquired with a Spot Insight QE digital camera using Spot software (V. 3.5) and processed in Adobe Photoshop version 7.0.

Phylogenetic reconstruction

BLAST analyses were used to identify human *HSPG2/Perlecan* (gi184426) as the protein containing Ig domains most similar to Sid4 and *Drosophila melanogaster* neural adhesion molecule Neuroglian/L1 (gi14286138) as most similar to Hemolin*s* from *Hyalophora cecropia* (gi2146896) and *Manduca sexta* (gi1346269). *Drosophila HSPG2* (gi21727889), zebrafish *L1* (gi36143027), *Heterodontus francisci* (horn shark) secreted immunoglobulin mu (gi70055) and *Homo sapiens* secreted Ig epsilon (gi70024) were included in the analysis. Protein sequences were aligned by ClustalW and evolutionary relationships reconstructed using the neighbor joining method (Saitou and Nei, 1987) (best tree option, uncorrected "p"; Macvector v. 7.2). Pairwise alignment was used to identify regions of highest similarity between Sid4 and mouse Perlecan/HSPG2. Sid4 signal peptide was excluded from this analysis.

Results

sid4 is a secreted IGSF

We identified a 1.146-kb mRNA expressed in 48 hpf embryonic zebrafish liver that encodes a predicted 382 amino acid protein (GenBank Accession AY494978). Comparison of Sid4 protein sequence to the NCBI Conserved Domain Database (v. 1.63) identified four Ig domains similar in sequence to those found in *Heparan Sulfate Proteoglycan-2* (HSPG-2/Perlecan) and neural cell adhesion molecule Neuroglian/L1 (Fig. 1A). The best available data indicate that zebrafish HSPG2 (ENSDART00000031997, Zv. 4) resides on chromosome 23 while *sid4* is found on linkage group 25. Sid4 contains a signal peptide for secretion, but no other conserved motifs.

Detailed analyses of Ig domain organization in vertebrate and arthropod proteins revealed strikingly conserved structural features in *sid4* and the insect innate immune protein

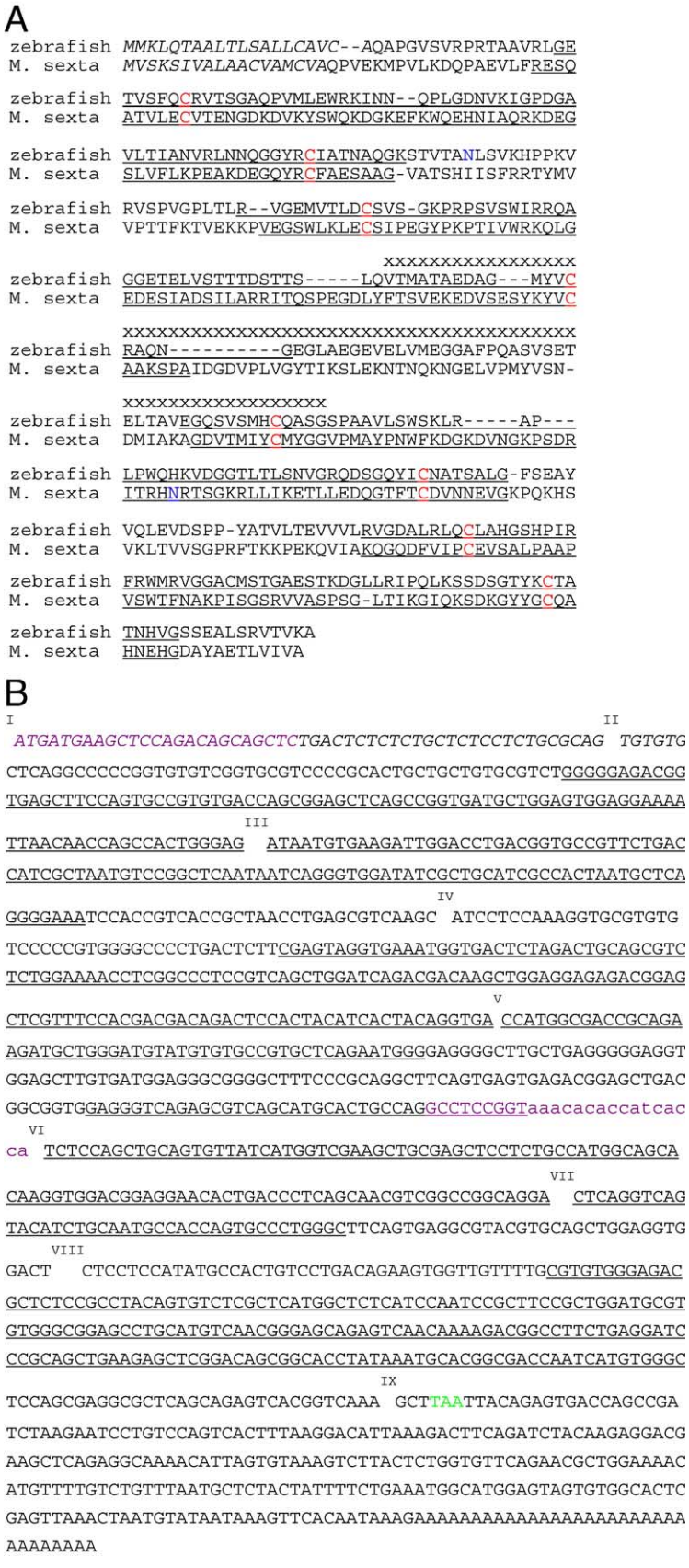
A
zebrafish MMKLQTAALTLSALLCAVC--AQAPGVSVRPRTAAVRLGE
M. sexta MVSKSIVALAACVAMCVAQPVEKMPVLKDQPAEVLFRESQ
zebrafish TVSFQCRVTSGAQPVMLEWRKINN--QPLGDNVKIGPDGA
M. sexta ATVLECVTENGDKDVKYSWQKDGKEFKWQEHNIAQRKDEG
zebrafish VLTIANVRLNNQGGYRCIATNAQGKSTVTANLSVKHPPKV
M. sexta SLVFLKPEAKDEGQYRCFAESAAG-VATSHIISFRRTYMV
zebrafish RVSPVGPLTLR--VGEMVTLDCSVS-GKPRPSVSWIRRQA
M. sexta VPTTFKTVEKKPVEGSWLKLECSIPEGYPKPTIVWRKQLG
xxxxxxxxxxxxxxxx
zebrafish GGETELVSTTTDSTTS-----LQVTMATAEDAG---MYVC
M. sexta EDESIADSILARRITQSPEGDLYFTSVEKEDVSESYKYVC
xxxxxxxxxxxxxxxxxxxxxxxxxxxxxxxxxxxxxxxxxx
zebrafish RAQN----------GEGLAEGEVELVMEGGAFPQASVSET
M. sexta AAKSPAIDGDVPLVGYTIKSLEKNTNQKNGELVPMYVSN-
xxxxxxxxxxxxxxxxx
zebrafish ELTAVEGQSVSMHCQASGSPAAVLSWSKLR-----AP---
M. sexta DMIAKAGDVTMIYCMYGGVPMAYPNWFKDGKDVNGKPSDR
zebrafish LPWQHKVDGGTLTLSNVGRQDSGQYICNATSALG-FSEAY
M. sexta ITRHNRTSGKRLLIKETLLEDQGTFTCDVNNEVGKPQKHS
zebrafish VQLEVDSPP-YATVLTEVVVLRVGDALRLQCLAHGSHPIR
M. sexta VKLTVVSGPRFTKKPEKQVIAKQGQDFVIPCEVSALPAAP
zebrafish FRWMRVGGACMSTGAESTKDGLLRIPQLKSSDSGTYKCTA
M. sexta VSWTFNAKPISGSRVVASPSG-LTIKGIQKSDKGYYGCQA
zebrafish TNHVGSSEALSRVTVKA
M. sexta HNEHGDAYAETLVIVA
B
I II
ATGATGAAGCTCCAGACAGCAGCTCTGACTCTCTCTGCTCTCCTCTGCGCAG TGTGTG
CTCAGGCCCCCGGTGTGTCGGTGCGTCCCCGCACTGCTGCTGTGCGTCTGGGGGAGACGG
TGAGCTTCCAGTGCCGTGTGACCAGCGGAGCTCAGCCGGTGATGCTGGAGTGGAGGAAAA
III
TTAACAACCAGCCACTGGGAG ATAATGTGAAGATTGGACCTGACGGTGCCGTTCTGAC
CATCGCTAATGTCCGGCTCAATAATCAGGGTGGATATCGCTGCATCGCCACTAATGCTCA
IV
GGGGAAATCCACCGTCACCGCTAACCTGAGCGTCAAGC ATCCTCCAAAGGTGCGTGTG
TCCCCCGTGGGGCCCCTGACTCTTCGAGTAGGTGAAATGGTGACTCTAGACTGCAGCGTC
TCTGGAAAACCTCGGCCCTCCGTCAGCTGGATCAGACGACAAGCTGGAGGAGAGACGGAG
V
CTCGTTTCCACGACGACAGACTCCACTACATCACTACAGGTGA CCATGGCGACCGCAGA
AGATGCTGGGATGTATGTGTGCCGTGCTCAGAATGGGGAGGGGCTTGCTGAGGGGGAGGT
GGAGCTTGTGATGGAGGGCGGGGCTTTCCCGCAGGCTTCAGTGAGTGAGACGGAGCTGAC
GGCGGTGGAGGGTCAGAGCGTCAGCATGCACTGCCAGGCCTCCGGTaaacacaccatcac
VI
ca TCTCCAGCTGCAGTGTTATCATGGTCGAAGCTGCGAGCTCCTCTGCCATGGCAGCA
VII
CAAGGTGGACGGAGGAACACTGACCCTCAGCAACGTCGGCCGGCAGGA CTCAGGTCAG
TACATCTGCAATGCCACCAGTGCCCTGGGCTTCAGTGAGGCGTACGTGCAGCTGGAGGTG
VIII
GACT CTCCTCCATATGCCACTGTCCTGACAGAAGTGGTTGTTTTGCGTGTGGGAGAC
GCTCTCCGCCTACAGTGTCTCGCTCATGGCTCTCATCCAATCCGCTTCCGCTGGATGCGT
GTGGGCGGAGCCTGCATGTCAACGGGAGCAGAGTCAACAAAAGACGGCCTTCTGAGGATC
CCGCAGCTGAAGAGCTCGGACAGCGGCACCTATAAATGCACGGCGACCAATCATGTGGGC
IX
TCCAGCGAGGCGCTCAGCAGAGTCACGGTCAAA GCTTAATTACAGAGTGACCAGCCGA
TCTAAGAATCCTGTCCAGTCACTTTAAGGACATTAAAGACTTCAGATCTACAAGAGGACG
AAGCTCAGAGGCAAAACATTAGTGTAAAGTCTTACTCTGGTGTTCAGAACGCTGGAAAAC
ATGTTTTGTCTGTTTAATGCTCTACTATTTTCTGAAATGGCATGGAGTAGTGTGGCACTC
GAGTTAAACTAATGTATAATAAAGTTCACAATAAAGAAAAAAAAAAAAAAAAAAAAAAA
AAAAAAAA

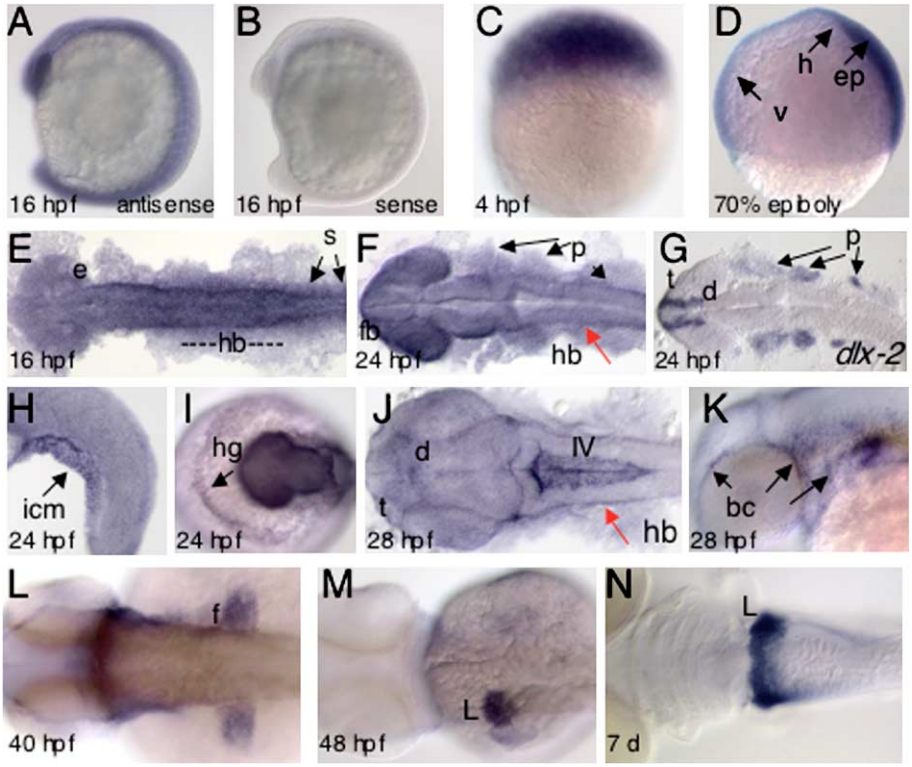

Fig. 2. *sid4* expression during normal zebrafish development. (A) Embryos hybridized to *sid4* antisense probe exhibited ubiquitous expression throughout early embryogenesis. (B) No signal was seen in embryos hybridized to the sense probe. (C) *sid4* is expressed throughout the blastoderm at 4 hpf and (D) in the hypoblast (h), epiblast (ep), and ventral blastomeres (v) of gastrulating embryos. (E) *sid4* is detected in the eye primordia (e), somites (s) and central nervous system of 16 hpf embryos. (F) *sid4* is expressed in the forebrain (fb), hindbrain (hb), eyes, and pharyngeal arch region (p) of 24 hpf embryos. (G) *dlx-2* expression is more restricted than *sid4* within the pharyngeal arch. (H) The inner cell mass (icm) and (I) hatching gland (hg) of 24 hpf embryos also express *sid4*. (J) *sid4* is absent from the 28-hpf hindbrain (red arrow) but prominently expressed in ventricle IV (IV), telencephalon (t), and diencephalon (d). (K) Scattered blood cells (bc) and (L) fin buds (fb) express *sid4* at 40 hpf. (M) By 48 hpf, sid4 is restricted to the liver, where it remains through 7 days of development (N). Lateral views in A–D; H, K. Dorsal views in E–G; J–N. Anterodorsal view in I. Embryonic stages are indicated at the lower left of each panel.

Hemolin (Fig. 1). Despite only 24% sequence identity, the two proteins are 66% similar when conservative substitutions are considered. The four Ig domains are similarly spaced in the zebrafish and insect proteins and each domain is flanked by conserved cysteine residues (Fig. 1A). Both *Hyalophora* Hemolin and Sid4 contain single, putative N-glycosylation sites (Fig. 1A). This modification occurs between domains 1 and 2 of *sid4* and within domain 3 of Hemolin (Su et al., 1998). Mature Hemolin forms a U-shaped horseshoe structure (Su et al., 1998) that places these glycosylation sites in very similar relative positions in the fully folded zebrafish and moth proteins.

From an analysis of contig sequences (Zv2 and 3), we found that the entire *sid4* coding region is contained in 9.75 kb of genomic sequence spanning 9 exons (Fig. 1B). Ig domains I–III of *sid4* are contained in exons 2–7. Like insect Hemolin, only the C-terminal Ig domain IV is encoded by a single exon (Fig. 1B). Sid4 is basic, with a pI of 8.62 and a predicted molecular weight of 38.3 kDa for the mature, processed protein.

sid4 is expressed in morphogenetically active cells during development

To identify tissues expressing *sid4* mRNA, we performed whole embryo in situ hybridization at selected stages of development. Expression at all stages analyzed by in situ was confirmed by standard RT-PCR (not shown). *sid4* mRNA was detected in embryos prior to the onset of zygotic gene expression (Fig. 2C). *sid4* was expressed throughout the blastoderm of gastrulating embryos (Fig. 2D) and this ubiquitous expression continued through 16 hpf, with elevated levels in the eye primordia, somites, and hindbrain (Fig. 2E). Expression in the 16 hpf hindbrain coincides with

Fig. 1. Zebrafish Sid4 and moth Hemolin exhibit similar Ig domain organization (A). Predicted Ig domains (underscored) were superimposed after sequence alignment. Signal peptides are italicized; conserved cysteines are in red; putative N-glycosylation sites are in blue. Overlying x denotes amino acids deleted by splice-inhibiting morpholino (B) *sid4* is encoded by nine exons (Roman superscripts) spanning 9.75 kb of genomic sequence. s-mo targets the exon5–intron5 boundary (uppercase and lowercase purple, respectively). t-mo targets the translationsal start site (purple). Signal peptide sequence is italicized and the first in-frame stop codon is in green.

the onset of cranial neural crest migration away from this region (Schilling and Kimmel, 1994).

By 24 hpf, *sid4* is widely expressed throughout the brain but is absent from the ventricles (Fig. 2F). Locally increased levels of *sid4* expression were also apparent in the 24 hpf trunk mesoderm, pharyngeal arch region (Fig. 2F), and inner cell mass (Fig. 2H). Within the prospective pharyngeal arch region, *sid4* is expressed in a broader, more continuous domain than the neural crest marker *dlx-2* (Fig. 2G) (Akimenko et al., 1994; Schilling and Kimmel, 1994). *sid4* is expressed in the hatching gland of the 24-hpf embryo (Fig. 2I), a highly migratory derivative of the prechordal mesoderm (Inohaya et al., 1997).

By 28 hpf, *sid4* expression is lost from the hindbrain but is strongly expressed in the telencephalon, diencephalon and ventricle IV of the hindbrain (Fig. 2J). At 40 hpf, expression of *sid4* is weaker in neural tissues, and transiently expressed in putative blood cells (Fig. 2K) and fin buds (Fig. 2L). *sid4* is detected in the liver by 48 hpf (Fig. 2M) and remains liver-specific through 7 days of development (Fig. 2N), a period of rapid expansion in organ size.

sid4 morpholino causes morphogenetic defects in developing embryos

To study the in vivo function of Sid4, we microinjected splice-inhibiting (s-mo) antisense morpholino oligonucleotides and their respective controls into single cell embryos. At the molecular level, we observed a reduction in size of the *sid4* RT-PCR product after injection of s-mo (Fig. 3A). Sequencing multiple clones of each indicated band confirmed deletion of exon 5 (not shown). Native *sid4* mRNA was detected in embryos injected with 100 μM *s-mo* but was absent from those injected with 150 μM (Fig. 3). The latter dose was used in all subsequent analyses. RNA isolated from s-co embryos also contained low levels of

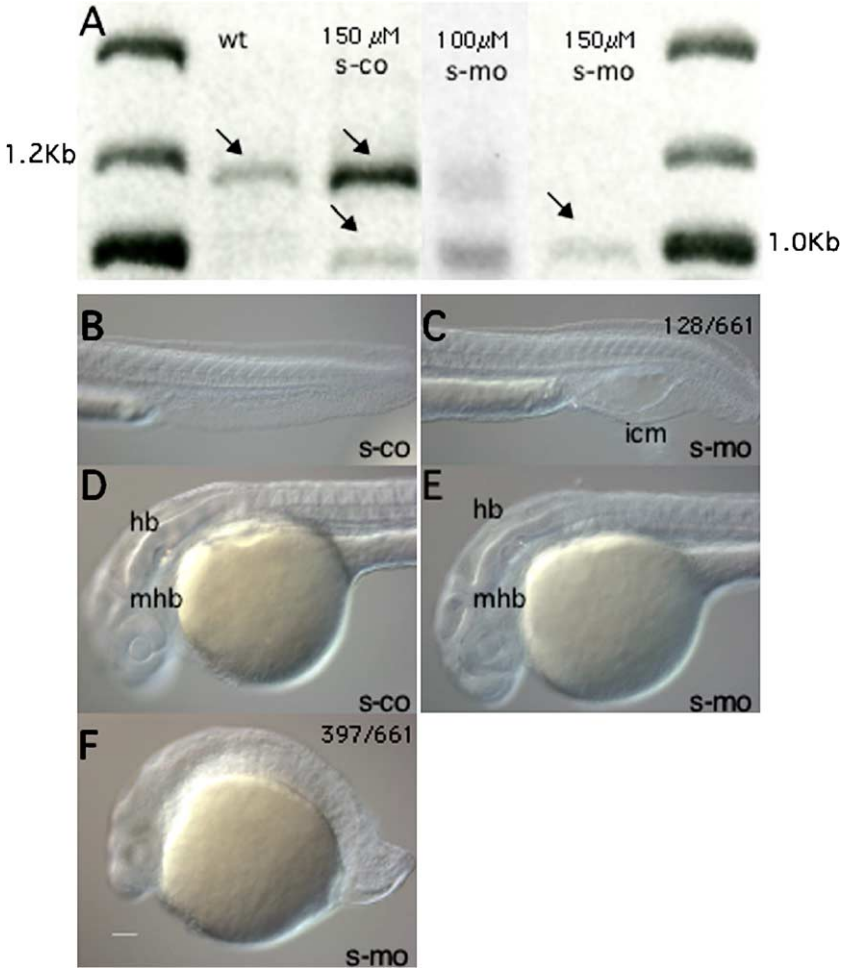

Fig. 3. Morpholino injection inhibits correct *sid4* mRNA splicing and disrupts development of mesoderm and neuroectoderm. (A) RT-PCR demonstrates dose-response s-mo-specific deletion of *sid4* exon 5. Treatments are given at the top of each lane. Arrows indicate amplification products that were cloned and sequenced. (B–G) Lateral views of live 24 hpf zebrafish embryos injected with 150 μM s-mo and s-co (B–F) and t-mo (G). (B) Tail mesoderm is unaffected by s-co. (C) Mildly affected morphant embryos exhibit expanded inner cell mass and defects in caudal somite morphology. Anterior somites appear normal. (D) Brain regionalization is normal in s-co and (E) mildly affected morphants. (F) In the majority of s-mo morphants, somites are rounded, tails severely truncated and brain structures indistinct. Magnification is the same in all panels. Anterior is to the left. hb, hindbrain; icm, inner cell mass; mhb, midbrain–hindbrain boundary.

exon-deleted *sid4,* suggesting that 5 bp mismatch still retains some affinity for *sid4* mRNA. Control embryos, however, never developed the morphological defects seen in morphants.

To assess the overall effect of *sid4* morpholinos on embryogenesis we examined the gross morphology of control and morphant embryos at 24 hpf. Morphants exhibited defects that ranged in severity. Mild morphants (19%) were normally sized and formed yolk extensions but displayed defects in the inner cell mass (ICM) and caudal trunk mesoderm (Fig. 3C). This defect appeared specific to caudal mesoderm because somites anterior to the ICM defect were normally shaped while more posterior somites were rounded at their antero-posterior boundaries (Fig. 3C). In comparison to controls (Fig. 3D), brain regionalization was morphologically normal in mild, 24 hpf s-mo morphants (Fig. 3E). The majority of s-mo morphants (60%) did not form yolk extensions, exhibited more severe posterior truncations and misshapen somites, and were much smaller than control embryos ("strong morphants", Fig. 3F). Brain regionalization of strong s-mo morphants was indistinct (Fig. 3F). The remaining s-mo morphants (21%) exhibited a range of intermediate defects (not shown).

sid4 MO affects morphogenesis but not differentiation

To understand the molecular and cellular bases for the defects in 24 hpf morphants, we examined gastrulation in live embryos and tissue formation by whole embryo in situ hybridization with tissue-and developmental stage-specific riboprobes.

Epiboly

During zebrafish epiboly the blastoderm migrates over the surface of the yolk, with the leading edge enclosing the yolk by 10 hpf. A subset of morphants (11%) exhibited prominent yolk extrusions, possibly due to premature constriction of the blastoderm (Figs. 4A, B). Comparable disruptions of epiboly and formation of yolk extrusions were produced by *sid4* s-mo (Fig. 4A) and t-mo (Fig. 4B), demonstrating that these defects are specific to attenuation of Sid4 protein activity. While these embryos likely represent a minority of morphants, their phenotypes suggest that abrogating Sid4 activity may alter the temporal relationship between yolk plug formation and active constriction at the blastoderm edge. The majority of morphants at this stage do not appear developmentally

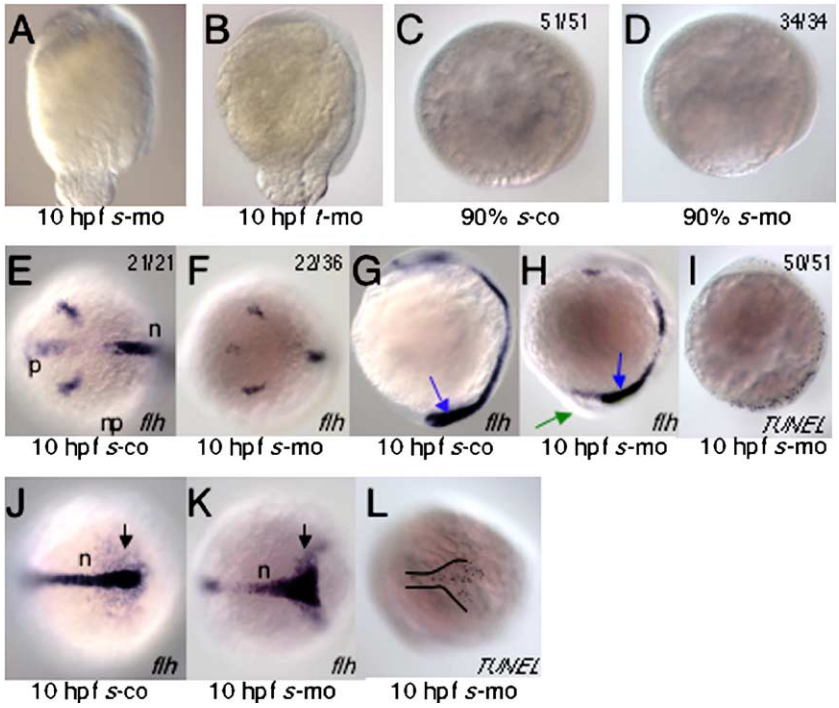

Fig. 4. *sid4* morpholinos cause morphogenetic defects and increased apoptosis. (A) s-mo and (B) t-mo produce similar epiboly defects. In these embryos, the blastoderm margin appears to constrict before the blastoderm completely covers the yolk. (C) Actively gastrulating control and (D) morphant embryos (90% epiboly) do not exhibit apoptosis. (E) *Flh* is appropriately expressed in the neural plate and polster of 10 hpf s-co and (F) s-mo embryos. The number of anterior *flh*+ cells appears reduced in the morphants. (G) *Flh*-expressing cells extend into the tail bud (blue arrow) of *s*-co embryos. (H) Yolk extrusions (green arrow) inhibit normal tail bud formation and patterning of caudal *flh*+cells. (I) Apoptosis increases in the caudal mesoderm of 10 hpf morphants. (J) Caudal *flh*-expressing cells (black arrows) converge normally and extend to form a narrow, compact notochord. (K) Convergence is impaired in morphant embryos and the notochord field is much broader than controls. (L) In many cases, the distribution of apoptotic cells in 10 hpf morphants was similar to *flh* expression patterns. Ratios of embryos exhibiting a given phenotype are in upper right. Lateral views in A–D; G–I. Dorsal views in E, F, J–L. Embryonic stages and treatments are indicated below each panel. In situ probes and TUNEL are indicated in lower right.

retarded because *flh* expression patterns (Fig. 4) are similar to normal 10 hpf embryos.

Axial mesoderm

We examined notochord formation in 10 hpf embryos using riboprobes to zebrafish *flh/floating head*, a marker of lateral neural plate, anterior prechordal mesoderm, and axial mesoderm/notochord (Melby et al., 1997; Talbot et al., 1995).

The *flh* expression pattern was normal in the lateral neural plate and polster of both control and morphant embryos (Figs. 4E–H). However, the numbers of anterior cells expressing *flh* appears reduced in morphants (Fig. 4F) and is consistent with the overall reduction in size of these embryos (Fig. 3F). Despite apparent reductions in cell number, the pattern of *flh* expression in morphants suggests that the spatial and temporal onset of anterior *flh* expression is normal.

Normally, caudal *flh*-expressing cells extend into the tailbud (Fig. 4G). Axial cells migrate normally to the shield and extend to form a compact, narrow notochord (Fig. 4J). In morphants, normal tail bud formation is disrupted (Fig. 4H) and caudal *flh*-expressing cells do not converge on the midline (Fig. 4K). The anterior notochord of morphants (Fig. 4K) was shortened and broader than that seen in controls (Fig. 4J). The formation of yolk extrusions in 11% of morphants only partially accounts for mispatterning of *flh*-expressing cells in 61% of mo-injected embryos and suggests that more subtle changes resulting from s-mo can cause defects in *flh* expression pattern.

One possible explanation for the reduced *flh* expression domains and overall body size was that *sid4* is required for cell survival. TUNEL analysis revealed no significant differences in levels of apoptosis in control (Fig. 4C) and morphant (Fig. 4D) embryos up to 90% epiboly. Because *sid4* is expressed from the earliest stages of development examined, it is unlikely that the changes in morphant *flh* gene expression at 10 hpf are due to apoptosis. It is likely, however, that apoptosis may contribute to reductions in cell number and overall body size later in development. In 10 hpf morphants, increased apoptosis was concentrated in the posterior of the embryo (Fig. 4I) and apoptotic cells were often distributed in patterns similar to morphant *flh* expression (Fig. 4L).

Somites and blood

Expression of zebrafish *unc45*, a gene expressed in developing muscle (Etheridge et al., 2002), was normal in 16 hpf control embryos (Fig. 5A). In contrast, somite morphogenesis was severely disrupted in 16 hpf morphants (Fig. 5B). In morphants, posterior somites that failed to converge on the midline were broadened and more diffusely organized than controls (Fig. 5B). However, this malformation of somites was also seen in somites anterior to the convergence defect (Fig. 5B). This suggests that defects in somite patterning may not be a consequence of the convergence defect, but these two aspects of morphant development may be due to a common mechanism. Injection of *sid4* mRNA (not shown; see below) and expression DNA (Fig. 5C; see below) failed to induce any specific morphological or gene expression defects.

Normal differentiation of red blood cells (RBCs) (Figs. 5D–F), another derivative of the ventral mesoderm, was unaffected in morphants (Figs. 5E, F). While RBCs are clearly located near the dorsal aorta and axial vein in control embryos (Fig. 5D), few cells were seen outside of the ICM in *s-mo* (Fig. 5E) and *t-mo* (Fig. 5F) morphants. Using Nomarski optics to study live embryos, we could see occasional circulating cells (not shown), suggesting that the failure of cells to enter circulation was not due to defective blood vessel formation or to the expanded ICM. Instead, it is more likely that expansion of the ICM results from the inability of RBCs to emigrate. This interpretation is supported by our observations of *sid4* expression in the ICM (Fig. 2H) and normal blood cells (Fig. 2K), but not vasculature, and is consistent with the observed aggregation of Hemolin-deficient hemocytes (Bettencourt et al., 1997) and increased neuronal adhesion in Beat1a-deficient fly embryos (Fambrough and Goodman, 1996; Pipes et al., 2001).

Prechordal mesoderm

Because *sid4* is ubiquitously expressed during early development, we expected s-mo injection to produce defects throughout the embryo. Our first approach was to test whether all mesodermal derivatives were equally affected by examining development of the pre-chordal mesoderm.

At 7 and 10 hpf anterior migration of *gsc*-(Figs. 5G, H) and *hgg1*-expressing cells (Figs. 5I, J) was similar in control and morphant embryos. However, while the anterior border of migration was unchanged in morphants (Figs. 5H, J), the lateral spreading of prechordal mesoderm characteristic of 10 hpf control embryos (Figs. 5K, M) was similarly inhibited in both s-mo and t-mo morphants (Figs. 5L, N), with *Hgg1*-expressing cells remaining as a single cluster in the midline. These observations suggest that, despite ubiquitous mRNA expression, *sid4* has distinct functions in axial and prechordal mesoderm at similar stages of development. Futher, Sid4 has temporally distinct functions during early migration and later anterolateral spreading of hatching gland cells. It is possible that these spatial and temporal shifts in early *sid4* function reflect dynamic expression of its ligand.

Sid4 morphants exhibit reduced eyes and brain development like Wnt signaling mutants (Miller-Bertoglio et al., 1999) but, like BMP signaling mutants, also have severely reduced somitic mesoderm (Dick et al., 2000). To determine whether Sid4 morphants are ventralized or dorsalized we examined expression of *bmp4* and *chordin*. The normal

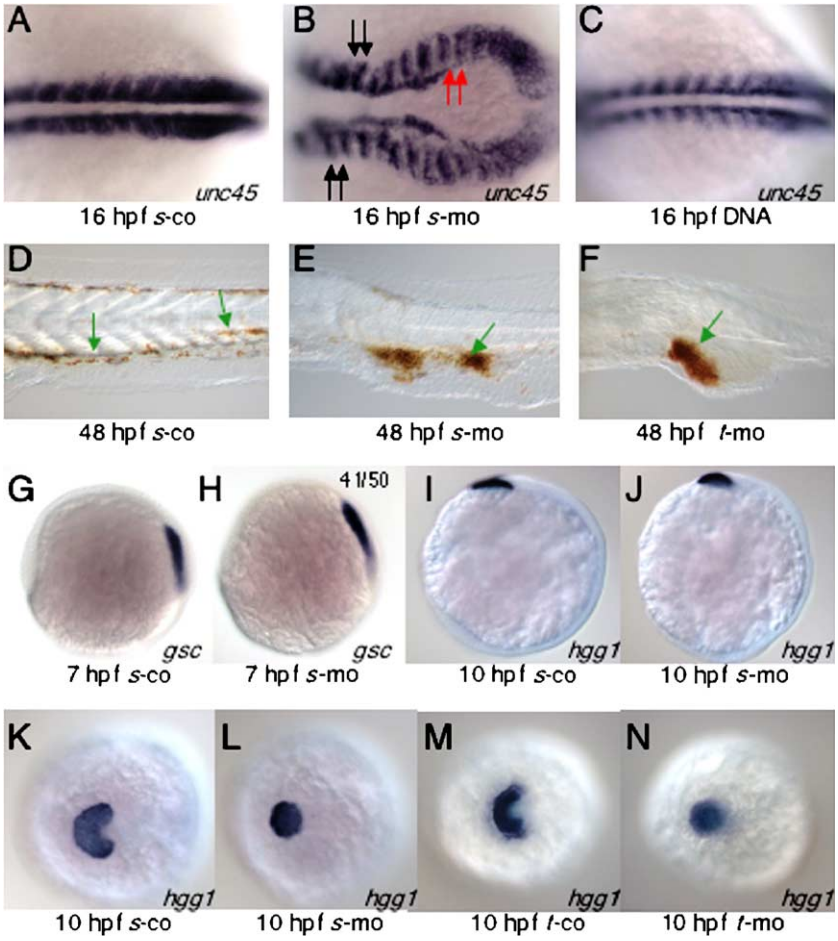

Fig. 5. Sid4 function during development of ventral and prechordal mesoderm. (A) In *s*-co embryos, somitic mesoderm develops normally. (B) Somite shape and convergence of caudal somitic mesoderm are disrupted in s-mo embryos. Somites anterior (black arrows) to and involved in (red arrows) the convergence defect are similarly malformed. (C) Somite development was normal in embryos injected with 25 pg/nl of *sid4* expression DNA. (D–F) Red blood cells stained with o-dianisidine. (D) Red blood cells can be seen within the vasculature of 24 hpf control embryos (green arrows). (E) In s-mo and (F) t-mo embryos, isolated red blood cells are seen in the proximity of blood vessels (green arrows), but the vast majority remain clumped within the abnormally expanded inner cell mass. (G) Anterior migration of *gsc*-expressing cells was similar in 7 hpf s-co and (H) s-mo embryos. (I) The anterior position of *hgg1* hybridization beneath the eye primordium of 10 hpf s-co and (J) s-mo embryos was also normal. (K) Lateral migration of hatching gland cells is normal in s-co and (M) t-co morphants. (L) In both 10 hpf s-mo and (N) *t*-mo morphants, hatching gland cells do not spread but remain in the midline. Embryonic stages and treatment are indicated below each panel. In situ probes are indicated at the lower right of each panel. Anterior is to the left. A–J are lateral views. K–N are anterodorsal views.

dorsal limits of *bmp4* expression (Fig. 6A) were unchanged in 6 hpf morphants (Fig. 6B), suggesting that, at this stage, Sid4 morphants are neither dorsalized nor ventralized. Likewise, *chordin* expression was similar in control (Fig. 6C) and morphant (Fig. 6D) embryos, suggesting that morphants retain normal domains of BMP activity. These data support our previous observations that, in morphants, early *goosecoid* and *hgg1* expression (Fig. 5) is normal and that early stage morphants are not apoptotic (Fig. 4).

sid4 MO affects neuroectoderm patterning but not cell differentiation

Early brain patterning

In 16 hpf wild type embryos, *Pax*-2 is expressed in the eye primordia and demarcates the midbrain–hindbrain boundary (MHB) (Krauss et al., 1991). The anterior–posterior (AP) patterning of *pax-2* expressing neural tissue was not altered in control (Fig. 7A) or morphant (Fig. 7B) embryos. As for *flh*, the number of *Pax2*-expressing cells in morphants is reduced (Fig. 7B). The AP pattern of *Krox-20* was normal in rhombomeres 3 and 5 of 14 hpf control (Fig. 7C) and morphant (Figs. 7D–F) embryos. However, rhombomeres were broader and the margins less well defined in 50% of morphants (Figs. 7D–F). In rare cases, cells forming rhombomere 5 did not converge on the midline (Fig. 7F). Since *chordin* expression is normal in early morphants (Figs. 6C, D), aberrant *krox20* expression may be due to failure of convergence.

Branchiomotor neurons

We further investigated the role of Sid4 in neural development by analyzing *Isl-1* expressing neurons in the hindbrains of *Isl-1*-GFP transgenic fish (Higashijima et al.,

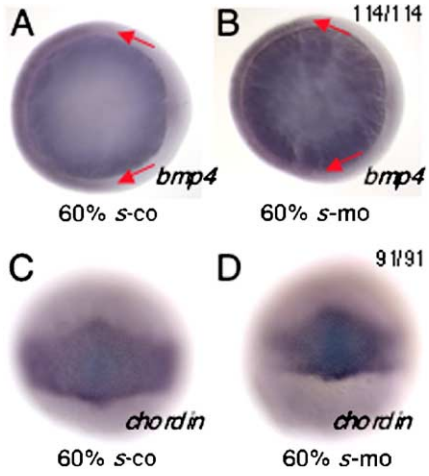

Fig. 6. Dorsal and ventral tissues of the zebrafish gastrula are normally patterned in *sid4* morphants. (A) The normal, dorsal margin of bmp4 expression is unchanged in (B) morphants. (C) No alterations of normal chordin expression were seen in (D) morphants. The light blue staining seen in C and D is a property of the BMP Purple substrate (Roche). Animal pole views in A, B; dorsal views in C, D. Embryonic stage is indicated below each panel. In situ probe is in lower right. Ratios of embryos exhibiting the phenotype are in the upper right.

2000). In 48 hpf control (Fig. 7G) and morphant (Figs. 7H, I) embryos, patterning of rhombomeres is normal and consistent with *krox20* expression. Specifically, the AP sequence of rhombomeres is normal in morphants but neurons are disorganized within rhombomeres (Figs. 7H, I). The close correspondence of 48 hpf Isl-1GFP and 14 hpf *krox*20 expression patterns suggests that apoptosis does not substantially contribute to this neural phenotype. Instead, as for zebrafish *trilobite* mutants, aberrant GFP expression in the hindbrain may be due to defective, caudal migration of neurons out of rhombomere 4 (Bingham et al., 2002; Chandrasekhar et al., 1997; Jessen et al., 2002). This would be consistent with our observations of defective migration in axial (Fig. 4) and prechordal (Fig. 5) mesoderm and with our sequence analysisthat suggests Sid4 mediates cellular interactions with the extracellular matrix (see below). As expected, the degree of neuronal disorganization was associated with the severity of tail truncation. More severe disorganization was seen in 19 severely truncated embryos, with the rest (17 embryos) either normal or exhibiting minor defects in patterning (not shown).

Cranial neural crest

Cranial neural crest is a highly migratory cell population that delaminates from the hindbrain and contributes to, among other tissues, the zebrafish eye, pigment cells, forebrain, and pharyngeal arch (Nissen et al., 2003; Schilling and Kimmel, 1994; Schilling et al., 1996). A role for *sid4* in cranial neural crest development was suggested by its prominent expression in these anatomical sites during development (Figs. 2C, D).

Patterns of non-retinal pigmented epithelium over the eye are normal in control embryos (Fig. 7J) but disrupted in

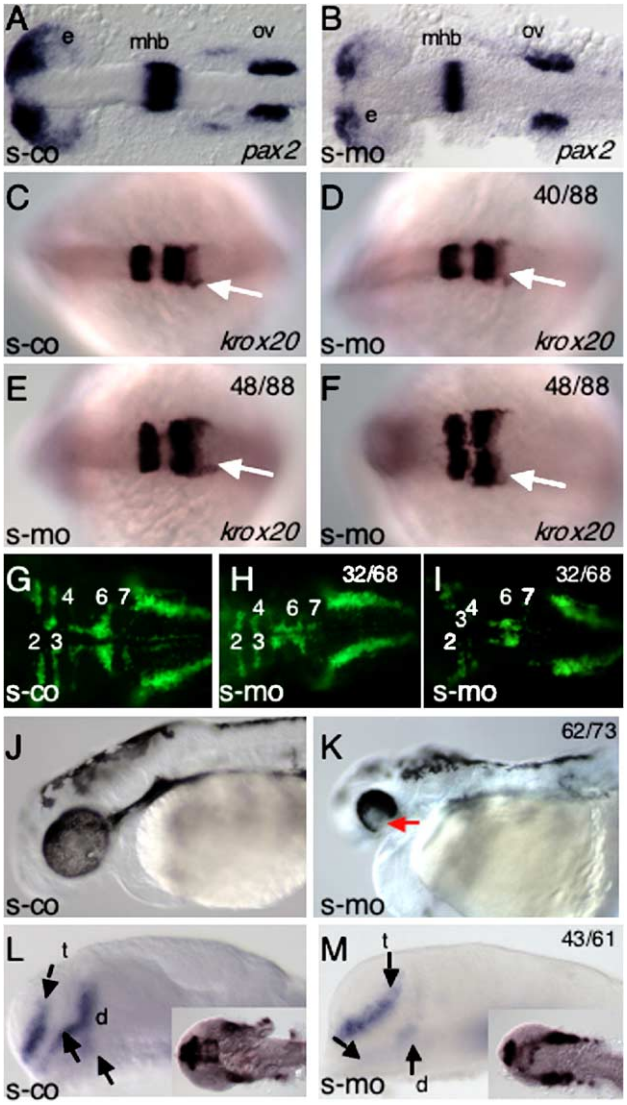

Fig. 7. *sid4* s-mo causes defects in local patterning of branchiomotor neurons and cranial neural crest development without altering early anteroposterior patterning of the brain. (A) The pattern of *pax-2* expression is normal in eye primordia, midbrain hindbrain boundary, and otic vesicles of both control and (B) morphant embryos, although the number of *pax-2* cells within each expression domain of morphants appears reduced. (C–F) The AP pattern of *krox20* expression in rhombomeres 3 and 5 and in migrating neural crest (white arrow) is unaffected in controls (C) and morphants (D–F). (E, F) Rhombomeres are broadened and boundaries more diffuse in morphants. (G) Branchiomotor neuron patterning is normal in control embryos but increasingly disorganized in (H) mildly affected and (I) caudally truncated embryos. (J) Normal migration of pigmented, non-retinal epithelium over the eyes of 48 hpf control embryos. (K) Pigment cells are concentrated in the dorsal portion of the eye in morphants (red arrow) and fail to migrate ventrally. (L) Normal forebrain expression of *dlx-2* in 24 hpf control embryos. (M) Diencephalic, *dlx-2* expressing neural crest cells are reduced or absent in morphants. This phenotype does not recover in 31 hpf embryos (insets in L, M). Dorsal views in A–I. Lateral views in J–M. Anterior is to the left in all panels. Embryos in J and K were fixed and cleared in glycerol. The right eye was removed and the left eye shown in both panels. d, diencephalon; e, eye; mhb, midbrain hindbrain boundary; ov, otic vesicle; t, telencephalon. In situ probes are indicated in the lower right of each panel.

morphants (Fig. 7K). This phenotype is remarkably uniform among morphants, with cells concentrated at the dorsal margin of the eye and a gap in pigmentation seen in the ventral and central portions of the eye (Fig. 7K). Morphant eyes are smaller than control (Figs. 7J, K), suggesting a possible role for cell death in this phenotype. However, the role of apoptosis in this phenotype is difficult to determine as it could begin at any stage after 90% epiboly and the effect could be cumulative. Morphants never exhibited cyclopia, suggesting that early expression of *sid4* in the eye primordia (Fig. 2C) was not related to separation of the two eye fields.

Functional Sid4 protein is also required for proper development of *dlx-2* expressing cells in the forebrain (Figs. 7L, M). *dlx2* is expressed in ventrally projecting stripes in both the telencaphalon and diencephalon of normal, 24 hpf embryos (Fig. 7L) (Akimenko et al., 1994). *sid4* mRNA is also expressed in these regions at 24 hpf. Anterior telencephalic neural crest appeared normal in morphants (Fig. 7M) but posterior staining was reduced or absent, demonstrating a loss of *dlx2*-expressing cells from the diencephalon. This effect could not be accounted for by developmental delay, as *dlx-2* expression in the morphant forebrain (Fig. 7M, inset) remains abnormal through 31 hpf (compare to 31 hpf controls in Fig. 7L, inset).

sid4 mRNA may be regulated at the level of stability

Despite numerous attempts, we were unable to rescue the morphant phenotype by co-injecting *sid4* mRNA. SDS-PAGE indicates that injecting 500 pg/nl of *sid4* mRNA produced no increase in Sid4 protein over that seen in uninjected controls (Fig. 8A). No signs of degradation were seen in concentrated *sid4* mRNA stocks or in mRNA left over after injection (Fig. 8B). In contrast, Sid4 protein was strongly expressed in embryos injected with the same DNA construct used for in vitro transcription (Fig. 8A). This suggests that mRNA derived from our plasmid constructs is competent for translation and that failure to translate directly injected mRNA may be due to in vivo degradation. This view is supported by our observation that Sid4 protein derived from DNA injection is also processed correctly. The newly synthesized protein migrates with a mass of 38 kDa, corresponding to the predicted MW of Sid4 after signal peptide cleavage. Thus, it seems likely that, although expressed throughout the embryo, *sid4* mRNA may be short-lived and tightly regulated in embryos. The high levels of Sid4 protein expressed from the DNA is likely due to the rapid replacement of mRNA by de novo transcription from the CMV promoter of pCS2.

Despite robust protein synthesis, we did not detect any morphological or gene expression phenotypes after injecting *sid4* expression DNA (Fig. 5C and data not shown). These data are similar to the lack of over/mis-expression reported for the Hox co-factors Meis and Pbx (Popperl et al., 2000; Vlachakis et al., 2001) and suggest that *sid4* may act as a co-factor.

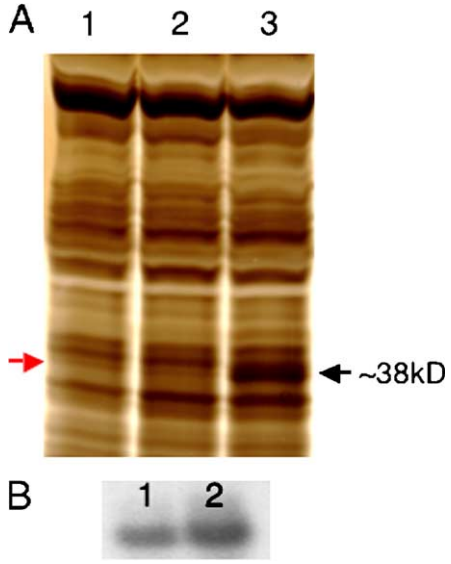

Fig. 8. *Sid4* protein synthesis in embryos injected with mRNA and DNA. (A) Protein extracts from 12 hpf uninjected controls (lane 1), and those injected with 500 pg/nl *sid4* mRNA (lane 2) exhibit similar amounts of Sid4 protein (red arrow). Robust Sid4 protein synthesis can be seen in extracts from embryos injected with 25 pg/nl pCS2*sid4* DNA (Lane 3, black arrow). This new protein migrates with a mass of ~38 kDa, the predicted size of Sid4 after signal peptide cleavage. (B) In vitro synthesized *sid4* mRNA retains its integrity during microinjection. Approximately 2 μg of pre-injection (lane 1) and post-injection (lane 2) mRNA was separated on standard 0.8% agarose gels and stained with ethidium bromide.

Phylogenetic analysis suggests a role for Sid4 in ECM interactions

Proteins with phylogenetically conserved functions often exhibit sequence or structural conservation. While Sid4 is structurally similar to Hemolin, its protein sequence is most similar to the vertebrate Perlecan/HSPG2, a major component of the ECM. We undertook detailed phylogenetic analysis to try to identify a possible role for Sid4 during development. Zebrafish Sid4 is most closely related to the adhesion-related Ig domains of human and *Drosophila HSPG2/Perlecan* (group 1) than to those of zebrafish *L1* and the structurally similar Hemolin (Fig. 9A) (Hughes, 1998), suggesting a role for Sid4 in interactions with the ECM. Alignment of Sid4 to the mouse Perlecan/HSPG2 sequence revealed striking sequence identity in the region of IG modules 7–12 (Hopf et al., 1999, 2001) (Fig. 9B). Sequence identity is particularly high to mouse amino acids 2566–2645, which are located within IG domains 10–12 (Hopf et al., 2001). This region of mouse Perlecan/HSPG2 is known to bind Fibronectin and Fibulin-2 (Hopf et al., 2001), important components of the extracellular matrix that mediate cellular adhesion, migration, and differentiation.

Discussion

Despite their molecular diversity and importance in physiology and embryonic development, few small, secreted immunoglobulin-containing proteins have been functionally characterized in vertebrates (Chiquet-Ehrismann and Chiquet, 2003; Sage and Bornstein, 1991; Sodek et al., 2002). In this paper we analyzed the embryological function of zebrafish *sid4*, which encodes a novel, secreted, vertebrate Ig protein. Our data suggest that Sid4 has important roles during vertebrate morphogenesis, possibly by mediating cellular interactions with the ECM.

sid4 morphants are phenotypically similar to several zebrafish mutants

During embryogenesis, *sid4* is expressed in multiple cell types undergoing rapid growth or migration. These include gastrulating axial and somitic mesoderm, prechordal mesoderm, eye primordia, and cranial neural crest. Intriguingly, *sid4* morphants are phenotypically similar to a number of

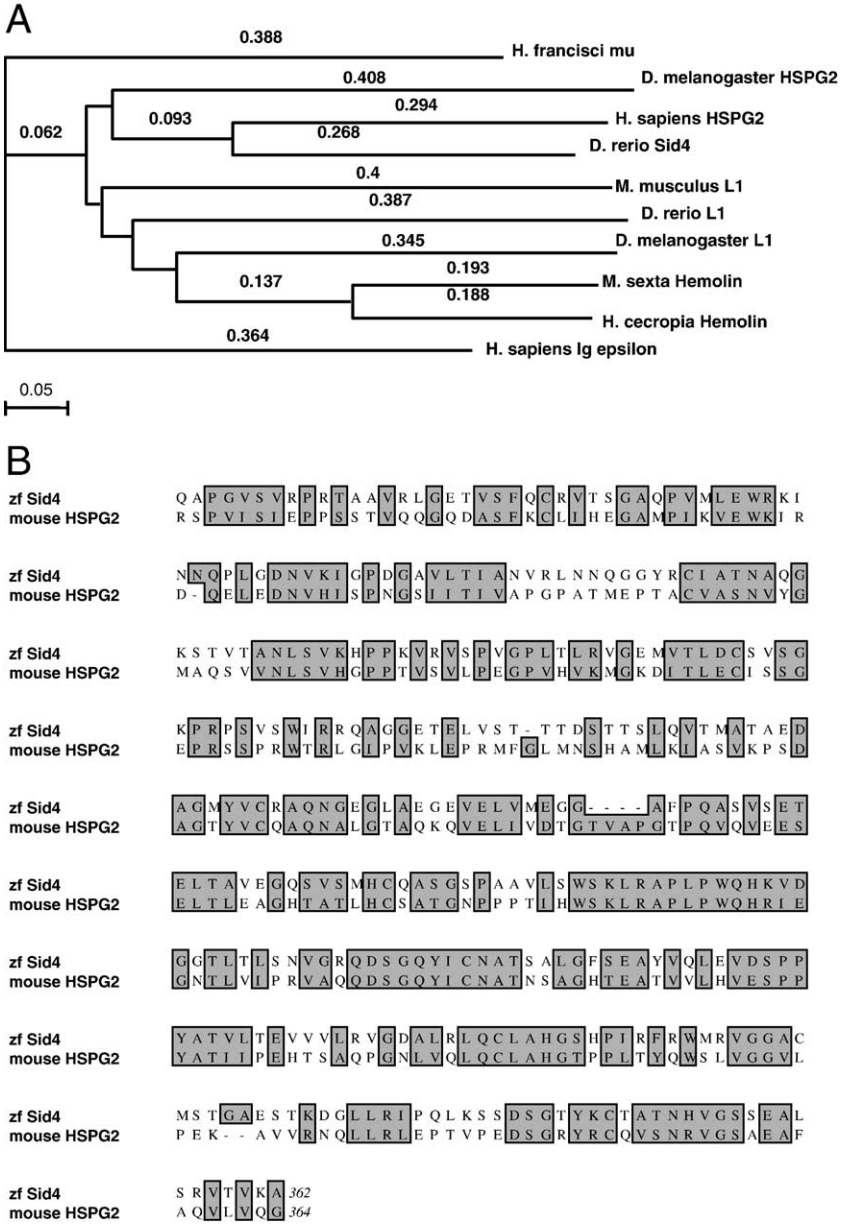

Fig. 9. Phylogenetic analysis suggests a role for Sid4 in mediating cellular interactions with the extracellular matrix. (A) Sid4 is most closely related to vertebrate and invertebrate *HSPG2* (group1) but more distantly related to Hemolin and L1 (group 2). The immunity-related horn shark Ig mu and human Ig epsilon served as out-groups. Numbers along each branch denote pairwise genetic distances (uncorrected "p"). (B) Sid4 is most similar to the fibronectin-binding Ig domains 10–13 (aa 2341–2705) of mouse HSPG2. Sid4 signal peptide was excluded from analysis. Shaded boxes highlight identical residues and conservative substitutions.

zebrafish mutants with diverse genetic bases. For example, *sid4* morphants exhibit severe loss of caudal, ventrally-derived mesoderm as found in BMP (Myers et al., 2002a) and FGF (Draper et al., 2003) signaling mutants. However, *bmp4* expression is normal in *sid4* morphants, suggesting that the ventral mesoderm of early embryos is correctly specified and patterned. Normal *chordin* expression in *sid4* morphants indicates that *bmp* signaling is also correctly regulated and further suggests that defects in this pathway do not underlie the mis-patterning of axial and somitic mesoderm.

The overall development of *sid4* morphant brain and eyes also resembles *prickle* (Wnt) morphants (Carreira-Barbosa et al., 2003; Veeman et al., 2003). Unlike *prickle* morphants, which exhibit delayed migration of prechordal mesoderm (Carreira-Barbosa et al., 2003; Veeman et al., 2003), the initial anterior migration of zebrafish *hgg1* expressing cells is normal. Morphants also exhibit broadening of somitic mesoderm, with loss of normal chevron-shaped somites, as seen in covergent extension mutants (Myers et al., 2002b). Strong *sid4* morphants exhibit failure of axial and somitic mesoderm to converge on the midline, but, unlike many convergent-extension mutants (Heisenberg and Nusslein-Volhard, 1997; Marlow et al., 1998), never exhibit cyclopia.

Sid4 morphants exhibit many characteristics of the epiboly mutants (Kane et al., 1996) and microtubule-defective embryos (Strahle and Jesuthasan, 1993). For example, strong *sid4* morphants exhibit defects in blastoderm migration and "yolk plug" closure. Failure of the blastoderm to fully enclose the yolk impairs convergence of the somitic mesoderm on the midline (Kane et al., 1996; Strahle and Jesuthasan, 1993). Only the most severe *sid4* morphants undergo true epiboly arrest and yolk lysis. Retraction of the blastoderm after arrest was not observed (Kane et al., 1996). The underlying genetics of delayed epiboly remain unclear. That Sid4 is a secreted protein with sequence similarity to extracellular matrix-binding domains suggests that defective cell–substrate interactions may contribute to delayed epiboly.

By a number of criteria, including gene expression (*gsc*, *hgg1*, *bmp4* and *chordin*) and TUNEL analysis, we found that early (up to 90% epiboly) *sid4* morphants were normal. Only during later gastrulation and tail bud formation did morphants exhibit changes in *flh*, *unc-45*, and *hgg1* expression. Further, increased apoptosis was seen in morphants from 90% epiboly onward, after the aberrant patterning of future notochord and somitic mesoderm was established. We interpret these data to mean that apoptosis does not contribute to the initial patterning of axial and somitic mesoderm but may account for the reduced numbers of cells expressing a particular marker and for the overall reduction in morphant embryo size. We believe that the most parsimonious explanation for the similarities and differences of *sid4* morphants to the zebrafish mutants may be that *sid4* participates in a process common to all of these mutants, such as adhesion or migration.

sid4 may function as a co-factor in a heterophilic process

Despite ubiquitous mRNA expression, *sid4* knockdown has distinct spatial and temporal effects in the early zebrafish embryo. For example, at similar developmental stages, morphogenesis of axial and somitic mesoderm is impaired while migration of prechordal mesoderm is normal. Further, *sid4* knockdown differentially affects later development of prechordal mesoderm, demonstrating a stage-specific function in a single tissue during periods of ubiquitous expression of *sid4*. These data suggest that 1) *sid4* translation may be temporally and spatially regulated or 2) *sid4* interacts with a protein(s) that are in low abundance or exhibit tissue-and stage-specific restricted expression. Thus, the availability of potential ligands may be saturated by endogenous levels of Sid4 expression during normal development. Scarcity of binding sites may explain why overexpression of *sid4* expression DNA does not produce any overt phenotype, even though injection of this construct yields abundant Sid4 protein. Intriguingly, similar explanations likely account for the lack of overexpression phenotypes seen for the essential Hox co-factors Pbx and Meis (Popperl et al., 2000; Vlachakis et al., 2001).

Sid4 is similar to the fibronectin-binding Igs of perlecan/HSPG2

A role for Sid4 in interactions with the ECM is suggested by phylogenetic analysis. Despite structural similarity to Hemolin, Sid4 is most closely related to insect and vertebrate Perlecan/HSPG2. Within mouse Perlecan/HSPG2, Sid4 is highly similar to Ig domains 10–13, a region of *HSPG2* known to bind Fibronectin and Fibulin-2 (Hopf et al., 1999), important components of the ECM. Given these observations, and the striking similarities of *sid4* morphants to Fibronectin- and Integrin β1-deficient *Xenopus* embryos (Marsden and DeSimone, 2003), we hypothesize that Sid4 may function as an adaptor molecule or as an anti-adhesive in cell–matrix interactions. Morpholino-induced disruption of Sid4 function may disrupt these interactions during gastrulation and lead to anoikis, or substrate-dependent cell death (Grossmann, 2002).

More detailed analyses of Sid4, including identification of potential ligands, extracellular localization and regulation by transcription factors are ongoing. These studies will add to a growing understanding of the molecular mechanisms by which a small, secreted immunoglobulin protein functions in vertebrate morphogenesis.

Acknowledgments

We thank A. Rossini, D. Greiner and J. Mordes for generous support. C. Sagerstrom, R. Bortell, R. Bettencourt, M. Ekker and D. Melton critically reviewed the data. Shannon Knuth (GeneTools) provided invaluable assistance

in morpholino design. This work was supported by the Diabetes and Endocrinology Research Center Grant 3P03-DK32520 from the National Institutes of Health and the Iacocca Foundation (P.J.D.).

References

Akimenko, M.A., Ekker, M., Wegner, J., Lin, W., Westerfield, M., 1994. Combinatorial expression of three zebrafish genes related to distal-less: part of a homeobox gene code for the head. J. Neurosci. 14, 3475–3486.

Barrallo-Gimeno, A., Holzschuh, J., Driever, W., Knapik, E.W., 2004. Neural crest survival and differentiation in zebrafish depends on mont blanc/tfap2a gene function. Development 131, 1463–1477.

Bettencourt, R., Lanz-Mendoza, H., Lindquist, K.R., Faye, I., 1997. Cell adhesion properties of hemolin, an insect immune protein in the Ig superfamily. Eur. J. Biochem. 250, 630–637.

Bettencourt, R., Gunne, H., Gastinel, L., Steiner, H., Faye, I., 1999. Implications of hemolin glycosylation and Ca2+-binding on homophilic and cellular interactions. Eur. J. Biochem. 266, 964–976.

Bettencourt, R., Terenius, O., Faye, I., 2002. Hemolin gene silencing by ds-RNA injected into Cecropia pupae is lethal to next generation embryos. Insect Mol. Biol. 11, 267–271.

Bingham, S., Higashijima, S., Okamoto, H., Chandrasekhar, A., 2002. The zebrafish trilobite gene is essential for tangential migration of branchiomotor neurons. Dev. Biol. 242, 149–160.

Carreira-Barbosa, F., Concha, M.L., Takeuchi, M., Ueno, N., Wilson, S.W., Tada, M., 2003. Prickle 1 regulates cell movements during gastrulation and neuronal migration in zebrafish. Development 130, 4037–4046.

Chandrasekhar, A., Moens, C.B., Warren Jr., J.T., Kimmel, C.B., Kuwada, J.Y., 1997. Development of branchiomotor neurons in zebrafish. Development 124, 2633–2644.

Chiquet-Ehrismann, R., Chiquet, M., 2003. Tenascins: regulation and putative functions during pathological stress. J. Pathol. 200, 488–499.

Dick, A., Hild, M., Bauer, H., Imai, Y., Maifeld, H., Schier, A.F., Talbot, W.S., Bouwmeester, T., Hammerschmidt, M., 2000. Essential role of Bmp7 (snailhouse) and its prodomain in dorsoventral patterning of the zebrafish embryo. Development 127, 343–354.

diIorio, P.J., Moss, J.B., Sbrogna, J.L., Karlstrom, R.O., Moss, L.G., 2002. Sonic hedgehog is required early in pancreatic islet development. Dev. Biol. 244, 75–84.

Draper, B.W., Stock, D.W., Kimmel, C.B., 2003. Zebrafish fgf24 functions with fgf8 to promote posterior mesodermal development. Development 130, 4639–4654.

Etheridge, L., diIorio, P.J., Sagerstrom, C.G., 2002. A zebrafish unc-45-related gene expressed during muscle development. Dev. Dyn. 224, 457–460.

Fambrough, D., Goodman, C.S., 1996. The *Drosophila* beaten path gene encodes a novel secreted protein that regulates defasciculation at motor axon choice points. Cell 87, 1049–1058.

Grossmann, J., 2002. Molecular mechanisms of detachment-induced apoptosis—Anoikis. Apoptosis 7, 247–260.

Heisenberg, C.P., Nusslein-Volhard, C., 1997. The function of silberblick in the positioning of the eye anlage in the zebrafish embryo. Dev. Biol. 184, 85–94.

Higashijima, S., Hotta, Y., Okamoto, H., 2000. Visualization of cranial motor neurons in live transgenic zebrafish expressing green fluorescent protein under the control of the islet-1 promoter/enhancer. J. Neurosci. 20, 206–218.

Hopf, M., Gohring, W., Kohfeldt, E., Yamada, Y., Timpl, R., 1999. Recombinant domain IV of perlecan binds to nidogens, laminin-nidogen complex, fibronectin, fibulin-2 and heparin. Eur. J. Biochem. 259, 917–925.

Hopf, M., Gohring, W., Mann, K., Timpl, R., 2001. Mapping of binding sites for nidogens, fibulin-2, fibronectin and heparin to different IG modules of perlecan. J. Mol. Biol. 311, 529–541.

Hughes, A.L., 1998. Protein phylogenies provide evidence of a radical discontinuity between arthropod and vertebrate immune systems. Immunogenetics 47, 283–296.

Hwang, S.P., Tsou, M.F., Lin, Y.C., Liu, C.H., 1997. The zebrafish BMP4 gene: sequence analysis and expression pattern during embryonic development. DNA Cell Biol. 16, 1003–1011.

Inohaya, K., Yasumasu, S., Araki, K., Naruse, K., Yamazaki, K., Yasumasu, I., Iuchi, I., Yamagami, K., 1997. Species-dependent migration of fish hatching gland cells that express astacin-like proteases in common [corrected]. Dev. Growth Differ. 39, 191–197.

Jessen, J.R., Topczewski, J., Bingham, S., Sepich, D.S., Marlow, F., Chandrasekhar, A., Solnica-Krezel, L., 2002. Zebrafish trilobite identifies new roles for Strabismus in gastrulation and neuronal movements. Nat. Cell Biol. 4, 610–615.

Kane, D.A., Hammerschmidt, M., Mullins, M.C., Maischein, H.M., Brand, M., van Eeden, F.J., Furutani-Seiki, M., Granato, M., Haffter, P., Heisenberg, C.P., Jiang, Y.J., Kelsh, R.N., Odenthal, J., Warga, R.M., Nusslein-Volhard, C., 1996. The zebrafish epiboly mutants. Development 123, 47–55.

Kanost, M.R., Zepp, M.K., Ladendorff, N.E., Andersson, L.A., 1994. Isolation and characterization of a hemocyte aggregation inhibitor from hemolymph of Manduca sexta larvae. Arch. Insect Biochem. Physiol. 27, 123–136.

Kimmel, C.B., Ballard, W.W., Kimmel, S.R., Ullmann, B., Schilling, T.F., 1995. Stages of embryonic development of the zebrafish. Dev. Dyn. 203, 253–310.

Kozak, M., 1987. An analysis of 5′-noncoding sequences from 699 vertebrate messenger RNAs. Nucleic Acids Res 15, 8125–8148.

Krauss, S., Johansen, T., Korzh, V., Fjose, A., 1991. Expression of the zebrafish paired box gene pax[zf-b] during early neurogenesis. Development 113, 1193–1206.

Marlow, F., Zwartkruis, F., Malicki, J., Neuhauss, S.C., Abbas, L., Weaver, M., Driever, W., Solnica-Krezel, L., 1998. Functional interactions of genes mediating convergent extension, knypek and trilobite, during the partitioning of the eye primordium in zebrafish. Dev. Biol. 203, 382–399.

Marsden, M., DeSimone, D.W., 2003. Integrin–ECM interactions regulate cadherin-dependent cell adhesion and are required for convergent extension in *Xenopus*. Curr. Biol. 13, 1182–1191.

Melby, A.E., Kimelman, D., Kimmel, C.B., 1997. Spatial regulation of floating head expression in the developing notochord. Dev. Dyn. 209, 156–165.

Miller-Bertoglio, V., Carmany-Rampey, A., Furthauer, M., Gonzalez, E.M., Thisse, C., Thisse, B., Halpern, M.E., Solnica-Krezel, L., 1999. Maternal and zygotic activity of the zebrafish ogon locus antagonizes BMP signaling. Dev. Biol. 214, 72–86.

Mongiat, M., Taylor, K., Otto, J., Aho, S., Uitto, J., Whitelock, J.M., Iozzo, R.V., 2000. The protein core of the proteoglycan perlecan binds specifically to fibroblast growth factor-7. J. Biol. Chem. 275, 7095–7100.

Myers, D.C., Sepich, D.S., Solnica-Krezel, L., 2002a. Bmp activity gradient regulates convergent extension during zebrafish gastrulation. Dev. Biol. 243, 81–98.

Myers, D.C., Sepich, D.S., Solnica-Krezel, L., 2002b. Convergence and extension in vertebrate gastrulae: cell movements according to or in search of identity? Trends Genet. 18, 447–455.

Nakamura, M., Baldwin, D., Hannaford, S., Palka, J., Montell, C., 2002. Defective proboscis extension response (DPR), a member of the Ig superfamily required for the gustatory response to salt. J. Neurosci. 22, 3463–3472.

Nissen, R.M., Yan, J., Amsterdam, A., Hopkins, N., Burgess, S.M., 2003. Zebrafish foxi one modulates cellular responses to Fgf signaling required for the integrity of ear and jaw patterning. Development 130, 2543–2554.

Oxtoby, E., Jowett, T., 1993. Cloning of the zebrafish krox-20 gene

(krx-20) and its expression during hindbrain development. Nucleic Acids Res. 21, 1087–1095.
Panicker, A.K., Buhusi, M., Thelen, K., Maness, P.F., 2003. Cellular signalling mechanisms of neural cell adhesion molecules. Front Biosci. 8, d900–d911.
Pipes, G.C., Lin, Q., Riley, S.E., Goodman, C.S., 2001. The Beat generation: a multigene family encoding IgSF proteins related to the Beat axon guidance molecule in *Drosophila*. Development 128, 4545–4552.
Popperl, H., Rikhof, H., Chang, H., Haffter, P., Kimmel, C.B., Moens, C.B., 2000. Lazarus is a novel pbx gene that globally mediates hox gene function in zebrafish. Mol. Cell 6, 255–267.
Rossant, J., Howard, L., 2002. Signaling pathways in vascular development. Annu. Rev. Cell Dev. Biol. 18, 541–573.
Rougon, G., Hobert, O., 2003. New insights into the diversity and function of neuronal immunoglobulin superfamily molecules. Annu. Rev. Neurosci. 26, 207–238.
Sage, E.H., Bornstein, P., 1991. Extracellular proteins that modulate cell–matrix interactions, SPARC, tenascin, and thrombospondin. J. Biol. Chem. 266, 14831–14834.
Saitou, N., Nei, M., 1987. The neighbor-joining method: a new method for reconstructing phylogenetic trees. Mol. Biol. Evol. 4, 406–425.
Schilling, T.F., Kimmel, C.B., 1994. Segment and cell type lineage restrictions during pharyngeal arch development in the zebrafish embryo. Development 120, 483–494.
Schilling, T.F., Walker, C., Kimmel, C.B., 1996. The chinless mutation and neural crest cell interactions in zebrafish jaw development. Development 122, 1417–1426.
Schulte-Merker, S., Hammerschmidt, M., Beuchle, D., Cho, K.W., De Robertis, E.M., Nusslein-Volhard, C., 1994. Expression of zebrafish goosecoid and no tail gene products in wild-type and mutant no tail embryos. Development 120, 843–852.
Schulte-Merker, S., Lee, K.J., McMahon, A.P., Hammerschmidt, M., 1997. The zebrafish organizer requires chordino. Nature 387, 862–863.
Sodek, J., Zhu, B., Huynh, M.H., Brown, T.J., Ringuette, M., 2002. Novel functions of the matricellular proteins osteopontin and osteonectin/SPARC. Connect. Tissue Res. 43, 308–319.
Strahle, U., Jesuthasan, S., 1993. Ultraviolet irradiation impairs epiboly in zebrafish embryos: evidence for a microtubule-dependent mechanism of epiboly. Development 119, 909–919.
Su, X.D., Gastinel, L.N., Vaughn, D.E., Faye, I., Poon, P., Bjorkman, P.J., 1998. Crystal structure of hemolin: a horseshoe shape with implications for homophilic adhesion. Science 281, 991–995.
Sun, S.C., Lindstrom, I., Boman, H.G., Faye, I., Schmidt, O., 1990. Hemolin: an insect-immune protein belonging to the immunoglobulin superfamily. Science 250, 1729–1732.
Talbot, W.S., Trevarrow, B., Halpern, M.E., Melby, A.E., Farr, G., Postlethwait, J.H., Jowett, T., Kimmel, C.B., Kimelman, D., 1995. A homeobox gene essential for zebrafish notochord development. Nature 378, 150–157.
Teichmann, S.A., Chothia, C., 2000. Immunoglobulin superfamily proteins in *Caenorhabditis elegans*. J. Mol. Biol. 296, 1367–1383.
Thisse, C., Thisse, B., Halpern, M.E., Postlethwait, J.H., 1994. Goosecoid expression in neurectoderm and mesendoderm is disrupted in zebrafish cyclops gastrulas. Dev. Biol. 164, 420–429.
Vaughn, D.E., Bjorkman, P.J., 1996. The (Greek) key to structures of neural adhesion molecules. Neuron 16, 261–273.
Veeman, M.T., Slusarski, D.C., Kaykas, A., Louie, S.H., Moon, R.T., 2003. Zebrafish prickle, a modulator of noncanonical wnt/fz signaling, regulates gastrulation movements. Curr. Biol. 13, 680–685.
Vlachakis, N., Choe, S.K., Sagerstrom, C.G., 2001. Meis3 synergizes with Pbx4 and Hoxb1b in promoting hindbrain fates in the zebrafish. Development 128, 1299–1312.
Vogel, A., Gerster, T., 1997. Expression of a cathepsin L gene in anterior mesoderm and hatching gland. Dev. Genes Evol. 206, 477–479.
Westerfield, M., 2000. The Zebrafish Book. A Guide for the Laboratory Use of Zebrafish (*Danio Rerion*). University of Oregon Press, Eugene.
Willett, C.E., Zapata, A.G., Hopkins, N., Steiner, L.A., 1997. Expression of zebrafish rag genes during early development identifies the thymus. Dev. Biol. 182, 331–341.
Yoder, J.A., Nielsen, M.E., Amemiya, C.T., Litman, G.W., 2002. Zebrafish as an immunological model system. Microbes Infect. 4, 1469–1478.